Available online at www.sciencedirect.com
ScienceDirect
Catalysis Today 124 (2007) 185–190
CATALYSIS TODAY
www.elsevier.com/locate/cattod

# Characterizations of platinum catalysts supported on Ce, Zr, Pr-oxides and formation of carbonate species in catalytic wet air oxidation of acetic acid

Jana Mikulová, Sylvie Rossignol, Jacques Barbier Jr.*, Daniel Duprez, Charles Kappenstein

*Laboratoire de Catalyse en Chimie Organique, LACCO UMR 6503, CNRS and Université de Poitiers, 40 Avenue du Recteur Pineau, 82022 Poitiers Cedex, France*

Available online 27 April 2007

**Abstract**

Catalytic wet air oxidation (CWAO) of aqueous solution of acetic acid (78 mmol $L^{-1}$) was carried out with pure oxygen (2 MPa) at 200 °C in a stirred batch reactor on platinum supported oxide catalysts (Pt/oxide, oxide = $CeO_2$, $Zr_{0.1}Ce_{0.9}O_2$, $Zr_{0.1}(Ce_{0.75}Pr_{0.25})_{0.9}O_2$ and $ZrO_2$). Platinum was loaded on oxides by impregnation (5 wt%), and then the catalysts were reduced under $H_2$. Homogenous dispersions of 2–3 nm metal crystallites were obtained. The catalytic activity depended on the ability of the support to resist to the formation of carbonates. $Ce(CO_3)OH$ species, determined by FT-IR and XRD, were rapidly formed during the CWAO reaction especially on mixed oxides. These carbonates were responsible to a drastic drop in catalytic performances. Amounts of carbonate species increase with the ability of the catalyst to transfer oxygen.


*Keywords:* Acetic acid; Cerium oxide; Catalytic wet air oxidation; Platinum; Praseodymium; Zirconium; Oxygen storage capacity

## 1. Introduction

Water pollution is a tremendous issue for the next decades. There are already many processes able to eliminate the great majority of the pollutants in water including wet air oxidation (WAO). This promising technique is particularly cost-effective for effluents with medium chemical oxygen demand (10 g $(O_2)$ $L^{-1}$ < COD < 150 g $(O_2)$ $L^{-1}$) such as industrial or urban wastewaters, when biological treatments (10 g $(O_2)$ $L^{-1}$ > COD) are ineffective, e.g., in case of toxic effluents and when the concentrations of substances are too low for the economy of incineration processes (COD > 150 g $(O_2)$ $L^{-1}$). However, efficient WAO treatments require an elevated temperature (120–360 °C) and a high pressure of air or $O_2$ (5–20 MPa). Major research efforts are currently underway to achieve the total oxidation of organic effluent in wastewaters under milder conditions in presence of homogeneous or heterogeneous catalysts. Catalytic wet-air oxidation (CWAO) has been recently reviewed [1–4]. To improve the oxidation process efficiency, supported noble metal (Pt, Ru, etc.) catalysts are developed [5]. Various supports are used such as active carbon [6] or oxides ($TiO_2$, $CeO_2$, etc.) [7]. The CWAO conversion rate is directly linked to the ability of molecular oxygen to be transferred from the gaseous phase to the metal crystallites of the catalyst. Under classical reaction conditions, the oxygen concentration in aqueous media never exceeds 3 g $L^{-1}$ (2 MPa of $O_2$ in gaseous phase) [8]. Consequently, oxygen is in sub-stoechiometry with respect to the pollutant concentration. Thus, one of the essential steps in the reaction pathway corresponds to the oxygen migration from the support to the metal particles [9].

Rare-earth oxides have been widely investigated as structural and electronic promoters to improve the activity, selectivity and thermal stability of catalysts. The most significant of the oxides of rare-earth elements in industrial catalysis is certainly $CeO_2$, which has potential uses for the removal of organics from wastewaters (CWAO), as an additive in red ox reactions [10]. The success of ceria and $CeO_2$-based materials is mainly due to the unique combination of an elevated oxygen transport capacity coupled with the ability to shift easily between reduced and oxidized states (i.e. $Ce^{3+}$–$Ce^{4+}$). Oxygen storage capacity (OSC) derives from the ability

* Corresponding author. Tel.: +33 549 454 831; fax: +33 549 453 499.
*E-mail address:* jacques.barbier.jr@univ-poitiers.fr (J. Barbier Jr.).

0920-5861/$ – see front matter 
doi:10.1016/j.cattod.2007.03.036

of $CeO_2$ to be easily and reversibly reduced to the several $CeO_{2-x}$ stoechiometries when exposed to $O_2$-deficient atmospheres. Even after loss of oxygen from its lattice and the consequent formation of a large number of oxygen vacancies, $CeO_2$ maintains its fluorite type structure. This also facilitates rapid and complete refilling of oxygen vacancies upon exposure of $CeO_{2-x}$ to oxygen, with recovery of $CeO_2$ [11].

The major drawback of an oxygen storage system based on pure ceria is related to thermal resistance and low-temperature activity [12]. The main catalyst formulations studied contain either ceria thoroughly mixed with $ZrO_2$ in solid solution [13,14], which can enhance the thermal stability of ceria without diminishing its high oxygen mobility, or ceria doped with other rare-earth or transition metal oxides, which heavily modify the kinetics of oxygen transport and more efficient redox processes are permitted at much lower temperatures. Of the rare-earth elements, praseodymium element is particularly suitable for making a solid solution with cerium atoms. Structure of $Pr_6O_{11}$ is fluorite type and the ionic radius of $Pr^{4+}$ ions is close to that of $Ce^{4+}$ ions. In previous studies it was found that thermally stable $Zr_{0.1}(Ce_{1-x}Pr_x)_{0.9}O_2$ mixed oxides ($x$ between 0 and 0.75) prepared by sol–gel present a fluorite-type structure [15]. Some Raman experiments evidenced the presence of oxygen vacancies (570 $cm^{-1}$) associated to praseodymium cations. Consequently, high OSC values appear to be the result of the presence of both cerium and praseodymium ions at the two state oxidation ($Pr^{3+}/Pr^{4+}$). Therefore, the addition of praseodymium atoms into zirconia–ceria oxides appears to be very promising for materials with high oxygen mobility [16]. The main objective of this study is to determine the relation between the oxygen storage capacities of platinum supported catalysts and their activities in acetic acid catalytic wet air oxidation. Several platinum supported catalysts are consequently prepared, on various supports ($CeO_2$, $Zr_{0.1}Ce_{0.9}O_2$, $Zr_{0.1}(Ce_{0.75}Pr_{0.25})_{0.9}O_2$ and $ZrO_2$). The catalysts are precisely characterized before and after reaction tests. Acetic acid was chosen as model reactant because it is well known as one of the most refractory product of CWAO and its oxidation is a rate determining step for catalytic oxidation of many organic compounds [17,18].

## 2. Experimental

### 2.1. Catalyst preparation

The supports employed for the catalysts and their abbreviations are reported in Table 1.

Table 1
Nomenclature of supports and 5 wt% Pt catalysts

| Supports | Abbreviations for supports | Abbreviations for 5 wt% Pt catalysts |
|---|---|---|
| $CeO_2$ | Ce | PtCe |
| $Zr_{0.1}Ce_{0.9}O_2$ | ZrCe | PtZrCe |
| $Zr_{0.1}(Ce_{0.75}Pr_{0.25})_{0.9}O_2$ | ZrCePr | PtZrCePr |
| $ZrO_2$ | Zr | PtZr |

$CeO_2$ was prepared by precipitation, $Zr_{0.1}Ce_{0.9}O_2$, $Zr_{0.1}(Ce_{0.75}Pr_{0.25})_{0.9}O_2$ and $ZrO_2$ compounds by sol–gel method; both in according to the procedure previously reported, using cerium and praseodymium nitrate and zirconium *n*-propoxide as precursors [15]. The samples were dried for 1 h at 60 °C in a sand bath, thereafter for 12 h at 120 °C in a ventilated oven and calcined under air for 5 h at 500 °C.

All the catalysts were prepared by impregnation and dry evaporation of 4.75 g of the support in a Buchi Roto-vapor with 25 mL of aqueous solution of $Pt(NH_3)_4(OH)_2$ (10 g Pt $L^{-1}$) as a metallic precursor salt and 8 mL of distilled water per gram of support. The concentration of the solution was calculated to obtain a metal content of 5 wt% which is an usual loading for these noble metal WAO catalysts. The catalysts were dried overnight at 120 °C and finally activated by a reduction under $H_2$ (20 mL $min^{-1}$) for 3 h at 350 °C to obtain platinum metal.

Whatever the samples, the metallic precursor introduction fixed the pH value of the solution containing the support. The pH was near 1.

### 2.2. Catalytic test

Catalytic wet air oxidation reactions were carried out in a 0.44 L Hastelloy C22 autoclave for 3 h (Fig. 1).

The reaction temperature was 200 °C. Aqueous solutions of acetic acid (160 mL; COD = 5 g $L^{-1}$ corresponding to (acetic acid) = 78 mmol $L^{-1}$) and 4 g $L^{-1}$ of catalyst were introduced into the reactor. After an initial purge of the autoclave under helium, the autoclave was heated up to the reaction temperature. The reaction starts after addition of 2 MPa of oxygen. The pressure is maintained constant during the experiment. Acetic acid conversion was measured by analyzing the effluent composition as a function of time. At appropriated intervals of time, liquid and gas aliquots were sampled and analyzed by GC and HPLC.

Gas phase was analyzed by a GC equipped with a catharometer. A Porapak Q packed column (diameter = 0.6 mm, length = 0.5 m) was used for the $CO_2$ separation from the gas phase. Hydrogen was chosen as carrier gas. Knowing the $CO_2$ partial pressure, total $CO_2$ content in the reactor is possible to determine by using specific calibration

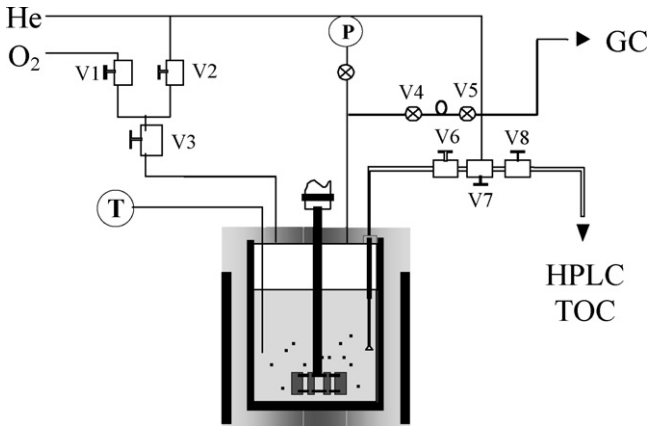


Fig. 1. Wet air oxidation reactor system.

charts presenting $CO_2$ in the gas phase versus $CO_2$ in the liquid phase [19]. In this study, $CO_2$ corresponds to the sum of the amounts of carbon dioxide in gas and liquid phases (soluble gas). This value takes into account the volumes of each phase in the reactor and is expressed in mol C $L^{-1}$ of solution.

Liquid samples were periodically drawn from the reactor and present components were identified by HPLC. Organic compounds were separated at 30 °C in $H_2SO_4$ (2 mmol $L^{-1}$) on an organic acid analysis column, Aminex HPX-87H (300× 7.8 mm) and analyzed by a diode array UV–vis detector (UV6000LP, Thermofinnigan) coupled with a refractive index detector (RI-150, Thermofinnigan).

The mineralization molar ratio ($M$) and the conversion of acetic acid ($C$) were also calculated. The mineralization $M$ molar ratio (Eq. (1)) corresponds to the ratio of the total $CO_2$ expressed in mol C $L^{-1}$ and the initial total organic carbon (in mol C $L^{-1}$):

$$M\,(\%) = \frac{CO_2}{TOC_i} \tag{1}$$

The conversion of acetic acid ($C$) is given by the decay of acetic acid concentration (mol $L^{-1}$) normalized to the initial concentration of this acid (Eq. (2)):

$$C\,(\%) = \frac{[\text{acetic}]_i - [\text{acetic}]_t}{[\text{acetic}]_i}. \tag{2}$$

### 2.3. Characterizations

BET specific surface areas of the samples were determined by adsorption of nitrogen at −196 °C in an automated Micromeritics ASAP 2000 apparatus after evacuation for 1 h 30 min at 350 °C. The method used is a simple BET 7 plots procedure between 0.05 and 0.25 values of $P/P_0$. The complete adsorption and desorption isotherms have been obtained for few samples, leading to the porous volume.

Diffractograms and particles size were determined by X-ray diffraction (XRD) experiments performed on a Siemens D 5005 powder $\theta$–$\theta$ diffractometer using the Cu Kα radiation ($\lambda_K$ = 0.154056 nm) and a graphite back-monochromator. XRD patterns were obtained under the following conditions: dwell time: 2 s; step: 0.04°; constant divergence slit: 1°. Crystalline phases were identified by comparison with PDF standards (powder diffraction files) from ICDD. The average crystallites sizes ($D$) are determined from the Scherrer equation (Eq. (3)):

$$D = \frac{K\lambda_K}{\beta \cos\theta} \tag{3}$$

$K$ = 0.9, $\lambda_K$ = 0.154056 nm, $\beta$ is the width at half maximum and $\theta$ is the Bragg angle for the considered peak (rad). For platinum only the peaks (1 1 1) and (2 2 0) have been taken into account.

Platinum crystallite sizes were obtained from transmission electron microscopy using a Philips CM 120 apparatus with a linear resolution of 3.5 Å.

FT-IR spectra were collected using a Perkin-Elmer spectrometer. The powder sample (10 mg) was dispersed in KBr (150 mg). Experimental conditions were: acquisition time = 120 s, number of scan = 20 and resolution = 4 $cm^{-1}$.

Hydrogen chemisorptions were carried out to determine the metal dispersion of the catalyst. This characterization has been performed in a chromatographic micro-reactor. After a reduction under $H_2$ (350 °C, 1 h) and a degassing under argon (350 °C, 3 h), some hydrogen pulses (0.26 mL) were injected at regular interval of time. Ultrapure $H_2$ and Ar (less than 1 ppm impurities) were used throughout this technique of characterization [20].

Oxygen storage capacity (OSC) was measured at 400 °C under atmospheric pressure. A 5 mg sample was continuously purged with helium (30 mL $min^{-1}$). Successive or alternate pulses (0.265 mL) of $O_2$ (Air Liquide, ≤5 ppm total impurities) and CO (Air Liquide, N20) were injected every 2 min [21]. The oxygen storage capacity (OSC) was calculated from the CO consumption after stabilization of the sample in alternate pulses condition.

## 3. Results and discussion

### 3.1. Characterizations of the fresh catalysts

#### 3.1.1. BET and crystallite size measurements

Specific area values of all supports are reported in Table 2. In agreement with previous studies [15], the results evidenced the zirconium as well as the praseodymium cations addition effect to ceria.

All final oxides present the same fluorite type structure except for $ZrO_2$ compound displaying a monoclinic, tetragonal and orthorhombic phase mixture as it was previously obtained [14]. Crystallite size of the catalyst supports (Table 2) shows that the addition of 5% weight of platinum does not significantly modify the structural data as well as the BET values which are very close. The measured dispersions and the calculated crystallite sizes determined by XRD and TEM are gathered in Table 3. All catalysts are in the dispersion range of 30–44%. Those results lead to crystallite sizes around 2–3 nm. TEM measurement of PtZrCe catalyst (Fig. 2) was given as an example of homogenous distribution of platinum crystallites. The difference in regard to the average crystallite size of platinum determined by TEM proves the presence of some large particles (XRD measurements). It can be due to overload of platinum, leading to the formation of particle agglomerates.

Table 2
BET surface area values of the supports and fresh catalysts and supports' crystallite sizes from XRD measurements (* phase mixture)

| Support | Ce | ZrCe | ZrCePr | Zr |
|---|---|---|---|---|
| Surface area ($m^2\ g^{-1}$) | 48 | 94 | 70 | 77 |
| Crystallite size (nm) | 17 | 8 | 9 | * |
| **Catalyst** | **PtCe** | **PtZrCe** | **PtZrCePr** | **PtZr** |
| Surface area ($m^2\ g^{-1}$) | 39 | 88 | 66 | 61 |
| Crystallite size (nm) | 16 | 8 | 9 | * |

Table 3
Dispersion and platinum crystallite size determined by chemisorption, XRD and TEM

| Catalyst | Pt dispersion[a] (%) | Crystallite size Pt (nm) | | |
|---|---|---|---|---|
| | | Chemisorption | XRD | TEM |
| PtCe | 39 | 2.4 | 38 | 1.5 |
| PtZrCe | 30 | 3.1 | 27 | 1.8 |
| PtZrCePr | 36 | 2.6 | 27 | 2.1 |
| PtZr | 44 | 2.1 | * | 1.7 |

* phase mixture, not calculated.
[a] $H_2$ chemisorption measurements.

Table 4
OSC measurements

| Catalyst | $D$ (%) | BET | $OSC_{meas}$[a] | $OSC_M$[b] | $OSC_{surf}$ | NL |
|---|---|---|---|---|---|---|
| Ce | – | 46 | 70 | 0 | 260 | 0.26 |
| ZrCe | – | 94 | 160 | 0 | 480 | 0.34 |
| ZrCePr | – | 70 | 280 | 0 | 360 | 0.79 |
| PtCe | 39 | 39 | 340 | 89 | 220 | 1.14 |
| PtZrCe | 30 | 88 | 810 | 78 | 450 | 1.62 |
| PtZrCePr | 36 | 66 | 840 | 94 | 330 | 2.30 |

[a] OSC measured at 400 °C ($\mu$mol $CO_2$ $g_{cat}^{-1}$).
[b] Number of O atoms necessary for a complete oxidation of accessible Pt atoms ($\mu$mol O $g_{cat}^{-1}$).

Moreover, the profile of platinum peaks can be attributed to different types of particles: (i) huge particles, responsible of the fine part of the peak, and (ii) smaller crystallites giving a widened aspect of the bottom of the peak (Fig. 4, fresh catalysts) [22]. Consequently, the XRD crystallite size calculation takes into account essentially the biggest crystallites.

### 3.1.2. OSC measurements

The OSC measurements are reported in Table 4 for the supports and the platinum based catalysts.

These results show clearly the beneficial effect of zirconium and praseodymium cations doping the OSC values as well for supports as catalysts. Moreover, the results confirm the positive effect of noble metal, which activates the oxygen atoms migration rate on the support [23].

To go further in the interpretations, the number of oxygen layers (NL, Eq. (5)) involved in the storage process is calculated on the basis of the theoretical number of reducible surface oxygen atoms ($OSC_{surf}$, Eq. (4)):

$$OSC_{surf} = \frac{bS}{Na^2} \quad (4)$$

$$NL = \frac{OSC_{meas} - OSC_M}{OSC_{surf}} \quad (5)$$

$S$ is the BET surface area ($m^2\ g^{-1}$), $a$ the lattice parameter (m), $N$ the Avogadro number and $b$ is the fraction of reducible elements (Ce + Pr) in the unit cell. This calculation is based on the following assumptions:

- All the $Ce^{IV}$ or $Pr^{IV}$ atoms of the surface monolayer are reduced to lower oxidation state (III).
- The surface faces are (1 0 0) and contain two metal atoms and four oxygen atoms per unit surface area $a^2$ ($a$ = cubic parameter); therefore one oxygen atom out of four participates to the OSC process as indicated by Eq. (4);
- Oxygen atoms bonded to reducible elements are the only one to participate to the OSC.

The NL values shows that while oxygen storage is limited to the surface of pure ceria, bulk oxygen atoms are involved in the case of mixed oxides; especially for the PtZrCePr catalyst. These results confirm that both Zr and Pr cations can change the kinetics of oxygen transport by enhancing redox processes. The insertion of these additives into $CeO_2$ leads to the lattice deformation, which generates higher mobility of oxygen atoms [24].

### 3.2. Catalytic results

The catalyst performances are given by their mineralization values in acetic acid oxidation, as shown in Fig. 3.

The highest mineralization is obtained for Pt catalyst supported over pure ceria. The catalysts based on mixed oxides

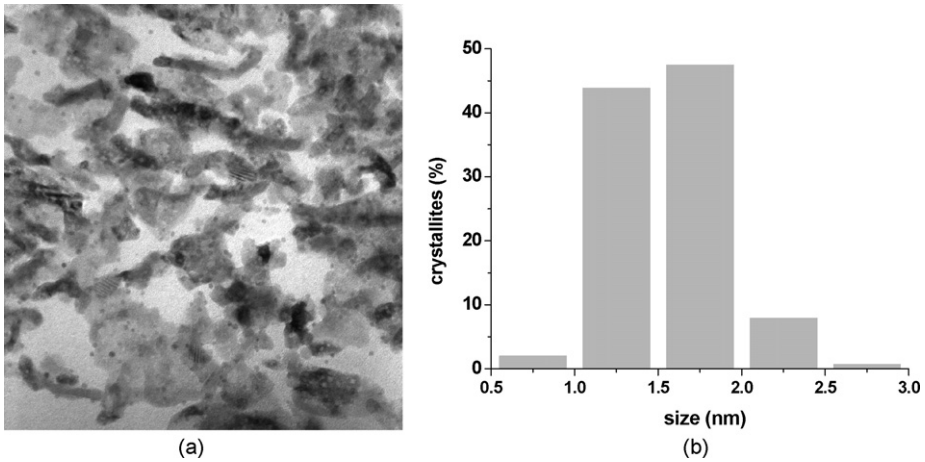


Fig. 2. TEM photo of PtZrCe (a) and distribution of platinum crystallite size (b).

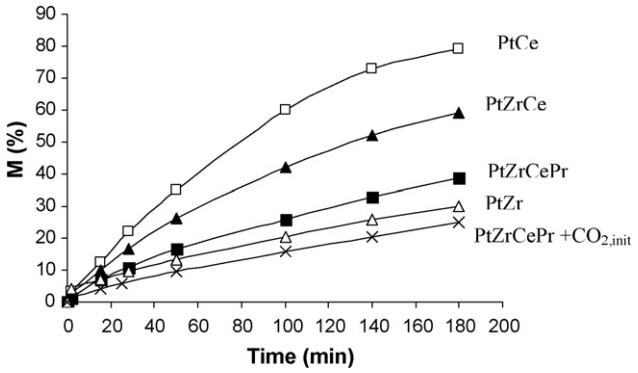


Fig. 3. Mineralization as a function of time for the various catalysts.

display lower activity rates. Surprisingly, taking into account the OSC values, the higher oxygen storage is, the lower the catalytic activity. A specific study, dealing with the $CO_2$ effect on catalytic activity, demonstrates clearly that an initial loading of $CO_2$ in the reactor (0.3 MPa, PtZrCePr + $CO_{2,init}$) decreases significantly the mineralization rate from the beginning of the run. To determine the inhibitor effect of $CO_2$, characterizations of used catalyzed were performed. XRD measurements of the bulk structure and FT-IR analyses, showing the surface adsorption phenomena, were carried out.

### 3.3. Characterizations of the catalysts after reaction

#### 3.3.1. X-ray diffraction

To determine the inhibitor effect of $CO_2$, XRD measurements have been performed on catalysts after the CWAO reaction. The fresh and used catalysts (after 2 and 180 min) are characterized (Fig. 4).

After 180 min of reaction, the diffractograms of PtZrCe and PtZrCePr samples show the presence of $Ce(CO_3)OH$ species (identified by *). Acetic acid, present in the medium, can react with ceria involving the formation of carbonate species and the reduction of cerium atoms (Eq. (6)). This can be attributed to privileged ability of cerium atoms to change its oxidation state in these mixed oxide supported catalysts [15]. The higher is the OSC values of the supports, the more significant the presence of carbonates is in the bulk. Consequently, for this type of catalysts, presented in this study and used in CWAO, the formation of carbonates seems to be correlated to the oxygen storage capacity:

$$CH_3COOH_{(l)} + 8CeO_{2(s)} \rightarrow 2Ce(CO_3)OH_{(s)} + 3Ce_2O_{3(s)} + H_2O_{(l)} \quad (6)$$

In the case of pure ceria the carbonaceous species are not supported on XRD patterns after reaction. However, after 2 min of reaction time, a very small line is observed on ceria catalyst. This catalyst seems to be able to eliminate these carbonates during the run contrary to what is observed on mixed oxides. It will be put forward that on ceria the reduction involve only on the surface and not in the bulk.

#### 3.3.2. FT-IR spectra

To be aware of the formation of carbonates, three samples (PtCe, PtZrCe and PtZrCePr) are analyzed by infrared spectroscopy. Fig. 5 illustrates the infrared spectra of these samples before catalytic reaction (fresh catalysts—(a)), after 2 min of reaction time (b) and after the end of the treatment running 180 min (c), including spectra of PtZrCePr after the reaction with initial loading of $CO_2$ (PtZrCePr + $CO_2$). A blank experiment performed on PtZrCe without acetic acid in the reactor is also presented.

Fig. 5a shows for all three fresh samples the bands corresponding to hydrogen carbonates ($\nu_{CO_3} = 1620$ and 1400 $cm^{-1}$), monodentate carbonates ($\nu_{CO_3} = 1500$ and 1350 $cm^{-1}$) as well as bidentate carbonates ($\nu_{CO_3} =$ 1570 and 1310 $cm^{-1}$) [25]. The highest amount of carbonate species possesses already as a fresh sample PtZrCePr

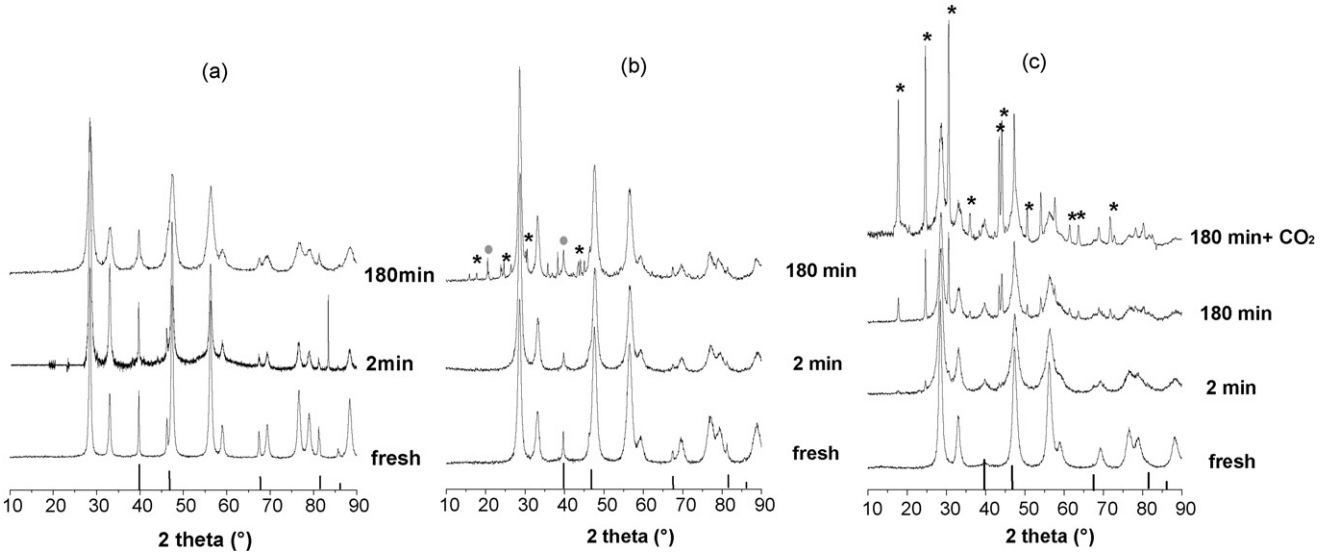


Fig. 4. X-ray patterns of the (a) PtCe, (b) PtZrCe and (c) PtZrCePr/PtZrCePr + $CO_{2,init}$ catalysts fresh, after 2 and 180 min CWAO reaction time (* PDF: 52-0352: $Ce(CO_3)(OH)$; — PDF: 04-0802: Pt).

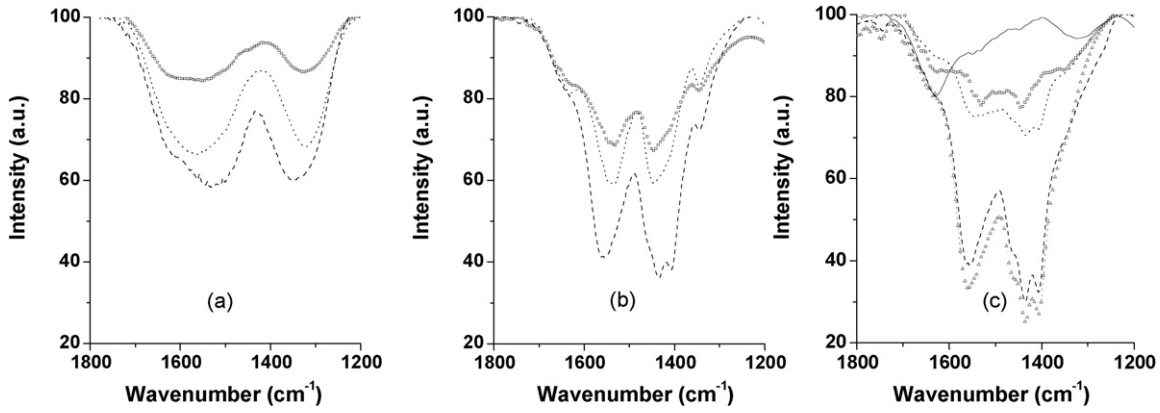


Fig. 5. FT-IR spectra of □: PtCe, ···: PtZrCe, - - -: PtZrCePr and △: PtZrCePr + $CO_2$, —: blank PtZrCe; fresh (a), after 2 min (b) and after 180 min (c).

compound. After the reaction, stopped at 2 min of reaction time, additional bands attributed to polydentate species ($\nu_{CO_3}$ = 1460, 1430 and 1410 $cm^{-1}$) are evidenced, prejudicial to those of hydrogen and monodentate carbonates. The bands corresponding to polydentate and bidentate species are even more pronounced at the end of catalytic reaction (180 min). It can be due to the change of temperature in agreement with other works announcing desorption of hydrogen carbonates (1620 $cm^{-1}$) since the temperature increases. Compare to the fresh and the used PtZrCe catalysts, the blank experiment reveals a low level of carbonates. This result proves that the $CO_2$ formed during the test is responsible of the new polydentate and bidentate band emergences.

Compared to pure ceria, the positions of all these bands shifts to lower frequency, which is due to the substitution of ceria by zirconium and praseodymium atoms. Detection of carbonates species confirms the presence of $Ce(CO_3)OH$ compound on XRD patterns after reaction. These results, especially in the presence of an initial loading of $CO_2$, indicate that the deactivation, which occurs during the first minutes of reaction, is induced by the presence of carbonates in the bulk as well as at the surface of the catalysts.

## 4. Conclusion

This work presents the characterizations and the catalytic wet air oxidation performances of platinum catalysts supported on various mixed oxides prepared by sol–gel method. $CeO_2$, $Zr_{0.1}Ce_{0.9}O_2$, $Zr_{0.1}(Ce_{0.75}Pr_{0.25})_{0.9}O_2$ and $ZrO_2$ are used as supports. Mixed oxides display the highest oxygen storage capacities. Platinum addition enhances efficiently the oxygen transfer on (and in) the catalytic support especially when Zr and Pr are added in the ceria structure. Using several methods of characterization of the fresh and used catalysts, it is demonstrated that the positive effect of these additions on OSC values are unfortunately responsible for a large formation of carbonates on the support in the presence of $CO_2$ which is the major by-product of acetic acid CWAO. These carbonates provoke a severe deactivation of catalysts. The high dispersion of platinum on the support induces very high transfer of oxygen in the bulk and seems to favour also the $CO_2$ migration. In order to understand and reduce this formation of carbonates, the influence of metallic crystallite sizes on $CO_2$ transfer is under study.

## References

[1] J. Levec, A. Pintar, Catal. Today 24 (1995) 51.
[2] F. Luck, Catal. Today 27 (1996) 195.
[3] F. Luck, Catal. Today 53 (1999) 81.
[4] S.V. Mishra, V.M. Mahajani, J.B. Joshi, Ind. Eng. Chem. Res. 34 (1995) 2.
[5] L. Oliviero, J. Barbier Jr., D. Duprez, Appl. Catal. B: Environ. 40 (2003) 163.
[6] L. Oliviero, J. Barbier Jr., D. Duprez, A. Guerrero-Ruiz, B. Bachiller-Baeza, I. Rodriguez-Ramos, Appl. Catal. B: Environ. 25 (2000) 267.
[7] A. Pintar, M. Besson, P. Gallezot, Appl. Catal. B: Environ. 31 (2001) 275.
[8] J. Barbier Jr., F. Delanoë, F. Jabouille, D. Duprez, G. Blanchard, P. Isnard, J. Catal. 177 (1998) 378.
[9] L. Oliviero, J. Barbier Jr., S. Labruquère, D. Duprez, Catal. Lett. 60 (1999) 15.
[10] A. Trovarelli, C. De Leitenburg, M. Boaro, G. Dolcetti, Catal. Today 50 (1999) 353.
[11] J. Zhang, Z.C. Kang, L. Eyring, J. Alloys Compd. 192 (1993) 57.
[12] S.J. Schmieg, D.N. Belton, Appl. Catal. B: Environ. 6 (1995) 127.
[13] J. Kaspar, P. Fornasiero, M. Graziani, Catal. Today 50 (1999) 285.
[14] S. Rossignol, Y. Madier, D. Duprez, Catal. Today 50 (1999) 261.
[15] S. Rossignol, C. Descorme, C. Kappenstein, D. Duprez, J. Mater. Chem. 11 (2001) 2587.
[16] S. Rossignol, D. Mesnard, F. Gerard, C. Kappenstein, D. Duprez, J. Mater. Chem. 13 (2003) 3017.
[17] H. Delvin, I. Harris, Ind. Eng. Chem. Fund. 23 (1984) 387.
[18] P. Gallezot, S. Chaumet, A. Perrard, P. Isnard, Catal. Today 168 (1997) 104.
[19] B. Renard, PhD Thesis of University of Poitiers, 2004.
[20] D. Duprez, J. Chim. Phys. 80 (1983) 487.
[21] S. Kacimi, J. Barbier Jr., R. Taha, D. Duprez, Catal. Lett. 22 (1993) 343.
[22] R.C. Koffi, C. Coutanceau, E. Garnier, J.-M. Léger, C. Lamy, Electrochim. Acta 50 (2005) 4117.
[23] S. Bedrane, C. Descorme, D. Duprez, Catal. Today 75 (2002) 401.
[24] G. Vlaic, P. Fornasiero, S. Geremia, J. Kaspar, M. Graziani, J. Catal. 168 (1997) 386.
[25] C. Binet, M. Daturi, J.-C. Lavalley, Catal. Today 50 (1999) 207.